Supporting Information: Free-energy landscape of polymer–crystal polymorphism

Chan Liu[1], Jan Gerit Brandenburg[2,3], Omar Valsson[1], Kurt Kremer[1], and Tristan Bereau[1,4]

[1]Max Planck Institute for Polymer Research, 55128 Mainz, Germany
[2] Interdisciplinary Center for Scientific Computing, University of Heidelberg, Im Neuenheimer Feld 205A, 69120 Heidelberg, Germany
[3] Digital Organization, Merck KGaA, Frankfurter Str. 250, 64293 Darmstadt, Germany
[4]Van 't Hoff Institute for Molecular Sciences and Informatics Institute, University of Amsterdam, Amsterdam 1098 XH, The Netherlands

August 12, 2020

1 Metadynamics

Metadynamics is an enhanced-sampling technique based on the addition of an adaptive external potential [1, 2]. Given the system's coordinates, $\boldsymbol{x}$, and its original potential energy, $U_0(\boldsymbol{x})$, we add to it a time-dependent bias potential, V, specified along specific collective variables (CVs), $\boldsymbol{z}(\boldsymbol{x})$. The resulting potential reads

$$U_b(\boldsymbol{x}, t) = U_0(\boldsymbol{x}) + V(\boldsymbol{z}(\boldsymbol{x}), t). \tag{S1}$$

Metadynamics implements a bias constructed from a sum of Gaussian functions centered on the visited points

$$V(\boldsymbol{z}(\boldsymbol{x}), t) = \sum_{t'} w(t') \exp\left(-\frac{|\boldsymbol{z}(\boldsymbol{x}(t)) - \boldsymbol{z}(\boldsymbol{x}(t'))|^2}{2(\delta \boldsymbol{z})^2}\right), \tag{S2}$$

where $w(t')$ scales the height of the Gaussian, $\delta\boldsymbol{z}$ is the Gaussian width, and $t' = \tau_{\mathrm{G}}, 2\tau_{\mathrm{G}}, \ldots$ is the time lag corresponding to adding Gaussians.

The bias potential will push the system to climb free-energy barriers along the CV space. Convergence of the method will lead to free diffusion of the system along the CVs. The bias potential thereby directly connects with the free energy via a time-dependent constant, $G(\boldsymbol{z}) = -V(\boldsymbol{z}, t) + c(t)$ [3].

The permanent addition of contributions to the bias potential typically leads to spurious fluctuations in the free energy. To mitigate this, well-tempered metadynamics [4, 5] proposes to tune the weight, w, as a function of time $w(t) = w_0 \tau_{\mathrm{G}} \exp\left(-V(\boldsymbol{z}, t)/k_{\mathrm{B}}\Delta T\right)$. This leads to a bias deposition rate that decreases like $1/t$. The parameter ΔT regulates the extent of the free-energy exploration.

We further use a reweighting method from Tiwary and Parrinello [6] to construct a time-independent estimator of the probability distribution of the CVs

$$P(\boldsymbol{z}) = P_b(\boldsymbol{z}) \mathrm{e}^{-\beta[V(\boldsymbol{z},t)-c(t)]}. \tag{S3}$$

The offset $c(t)$ is determined from

$$c(t) = \frac{1}{\beta} \ln \frac{\int \mathrm{d}\boldsymbol{z} \exp\left[\frac{\gamma}{\gamma-1}\beta V(\boldsymbol{z}, t)\right]}{\int \mathrm{d}\boldsymbol{z} \exp\left[\frac{1}{\gamma-1}\beta V(\boldsymbol{z}, t)\right]}, \tag{S4}$$

where $\gamma = \frac{T+\Delta T}{T}$ is the so-called biasing factor.

2 Collective variables

The efficiency of Metadynamics is strongly influenced by the choice of the CVs. Ideally the CVs should satisfy three properties [7]:

1. In the CV space, metastable states and transition states must be clearly distinguished as separate regions.

2. The CV space must not contain hidden barriers which are important for transitions and can describe all relevant "slow" processes.

3. The CVs should be limited in numbers, otherwise it will lead a high-dimensional space and take a considerable time to fill the free energy surface.

2.1 Unbiased simulations

In practice, a preliminary evaluation about the first requirement (distinguishability) is often made from the unbiased MD simulations. These runs are short enough that significant changes of crystalline structure are unlikely to occur.

Here we choose five phases, e.g., α, β, mix-1, mix-2 and amorphous. α and β are the main stable phases observed in experiments, while mix-1 and mix-2 are the intermediate phases (see Fig. S1).

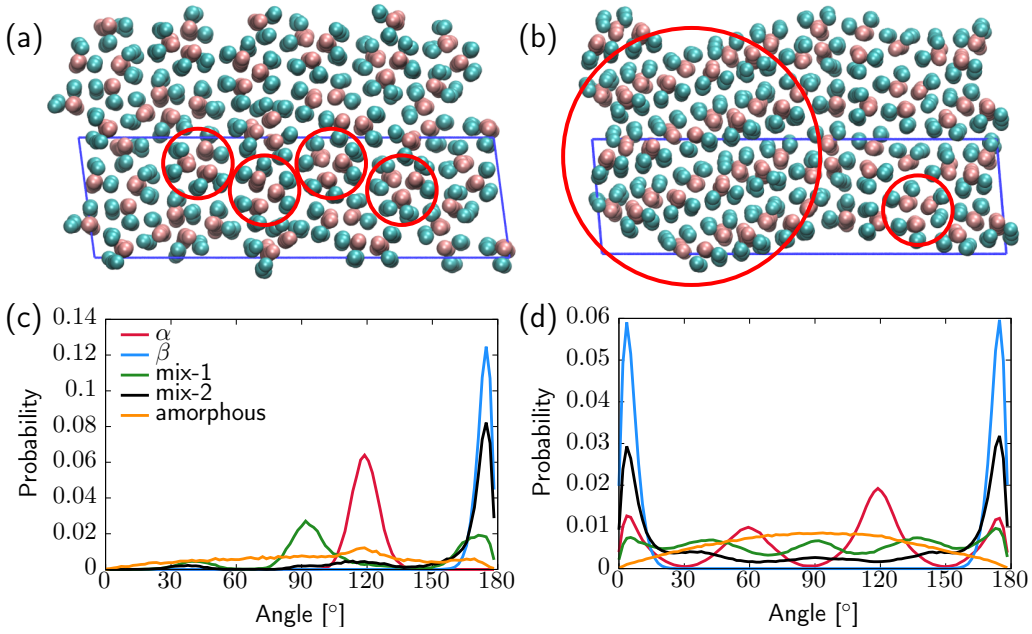

Figure S1: (a) mix-1 phase, (b) mix-2 phase, where mix-1 is close to α phase and mix-2 is close to β. (c)(d) Angle distributions between transverse vectors, $\boldsymbol{v}_2$, for five different phases: α, β, mix-1, mix-2, and amorphous. (c) 0.75 nm cutoff; (d) 3.0 nm cutoff.

The figure shows two different cutoffs, up to which we compute the angle distributions: 0.75 nm and 3.0 nm. The small cutoff, which only considers the nearest pairs, leads to distributions for α and β containing a single peak, and an amorphous amorphous phase that is virtually flat. The angle distribution of mix-1 features two main peaks centered at 90° and 180°, while mix-2 yields a single peak, analogous to β. The longer cutoff, which includes a second set of neighbors, leads to more peaks in the different distributions.

2.2 Legendre polynomial P_2

In Fig. S2 (a) and (b), we compare for each phase the time evolution of P_2 applied to the longitudinal vector $\boldsymbol{v}_1$, $P_2(\boldsymbol{v}_1)$, and the transverse vector $\boldsymbol{v}_2$, $P_2(\boldsymbol{v}_2)$. As illustrated in Fig. 1 of the main text, both vectors are constructed from intra-chain contributions, but only $\boldsymbol{v}_2$ can probe inter-chain geometries. Unsurprisingly, we find that $P_2(\boldsymbol{v}_1)$ can only separate between amorphous and crystalline phases, but not among them. Turning to $P_2(\boldsymbol{v}_2)$ instead, we find a much better separation of the different phases.

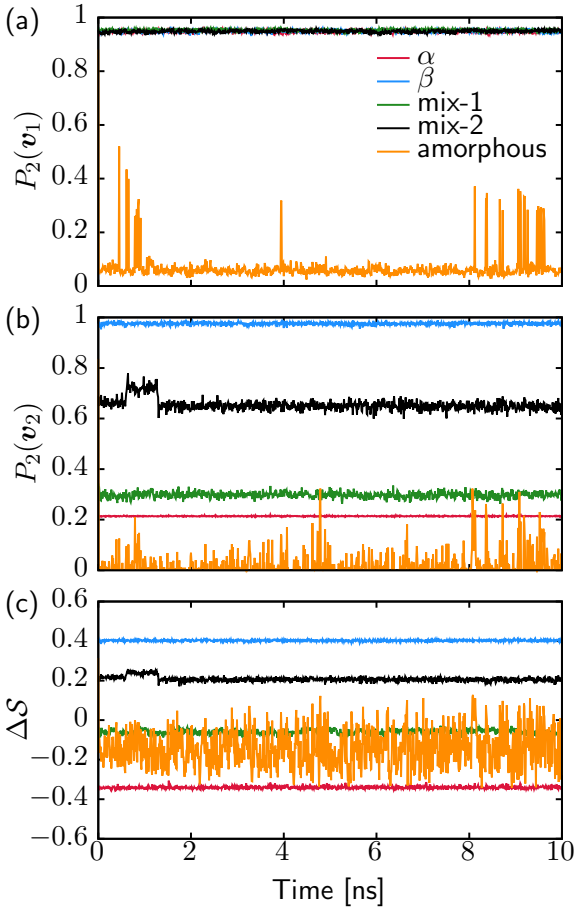

Figure S2: Time evolution of various CVs monitoring different phases from unbiased MD simulations. (a) P_2 order parameter applied to the longitudinal vector, $\boldsymbol{v}_1$; (b) P_2 applied to the transverse vector $\boldsymbol{v}_2$; (c) SMAC $\Delta\mathcal{S} = \mathcal{S}_\beta - \mathcal{S}_\alpha$.

2.3 SMAC

In Figure S2 (c), it is clear that this $\Delta\mathcal{S}$ can significantly distinguish the four crystalline phases, which can play a vital role in observing the pathway between α and β phases.

Table S1: Parameters used for the CVs used in this work: SMAC and $P_2(\boldsymbol{v}_2)$. Multiple entries in θ_n correspond to a simultaneous monitoring of several reference angles. Additionally, $\Delta\mathcal{S}$ is constructed from the CVs for α and β: $\Delta\mathcal{S} = \mathcal{S}_\beta - \mathcal{S}_\alpha$.

CV	r_σ [nm]	r_Ψ [nm]	θ_n [°]	σ_n [°]
$\mathcal{S}_\alpha$	0.75	3.0	120	25
$\mathcal{S}_\beta$	0.75	3.0	170	25
$\mathcal{S}_1$	3.0	3.0	0; 120; 170	12
$\mathcal{S}_2$	3.0	3.0	65; 120	25
$\mathcal{S}_3$	0.75	3.0	120; 170	12
$P_2(\boldsymbol{v}_2)$	3.0	–	–	–

2.4 Steinhardt parameter Q_6

Steinhardt parameters [8, 9] are order parameters that can describe the spherical symmetry of the system. They quantify orientational order using spherical harmonics computed on the polar angles of each bond in the system. Here, the bond is not a covalent bond but simply a vector connecting two beads within a pre-defined coordination radius.

The Steinhardt parameter Q_6 for each particle is a vector whose components are calculated using the following formula:

$$\boldsymbol{q}_{6m}(i) = \frac{\sum_j \sigma(r_{ij}) \boldsymbol{Y}_{6m}(\mathbf{r}_{ij})}{\sum_j \sigma(r_{ij})}, \tag{S5}$$

where $\{\boldsymbol{Y}_{6m}\}$ are the 6th order spherical harmonics and m runs from -6 to $+6$. With Steinhardt parameter, we do not associate a direction with a particular "bond", but project all vectors onto even spherical harmonics.

We calculate the mean of the vectors $\boldsymbol{q}_{6m}(i)$ and then take the norm of the resulting mean vector, which is called "vmean". Figure S3 shows that with vmean of Q_6, we can separate amorphous and mixture phases from α and β phases. Unfortunately, α and β phases seem to have the same degree of symmetry and cannot be distinguished.

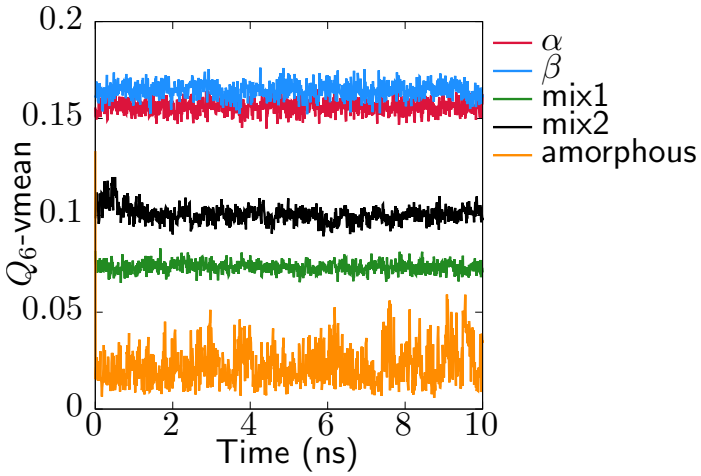

Figure S3: The time evolution of Q_6-vmean, i.e., taking the norm of the mean vector.

3 Two-dimensional metadynamics

3.1 $\Delta\mathcal{S}$ & Q_6

In Figure S4 (a), the α, β and mixture phases are indeed separated clearly. However, no transitions between α and β forms are observed with this CV-space (Figure S4 (b)(c)). We observed no transition within 200 ns of simulations. This strongly suggest that the set of CVs is inappropriate, hiding significant barriers.

3.2 Q_6 & $P_2(\boldsymbol{v}_2)$

A Metadynamics simulation showed no transition between the α and β phases (data not shown).

4 Free-energy profiles as a function of system size

Figure S5 compares the 1D projection of the free-energy surface along $\Delta\mathcal{S}$ for two types of size changes: (i) Number of monomers per chain and (ii) number of chains. Both variations lead to consistent profiles. In light of sampling challenges, we adapted the simulation temperature to facilitate convergence. Simulation time and temperature of each system simulation:

- $N^{\text{mon}} = 10$, $N^{\text{chain}} = 12$: temperature $T = 400$ K, simulation time $t = 3$ μs.

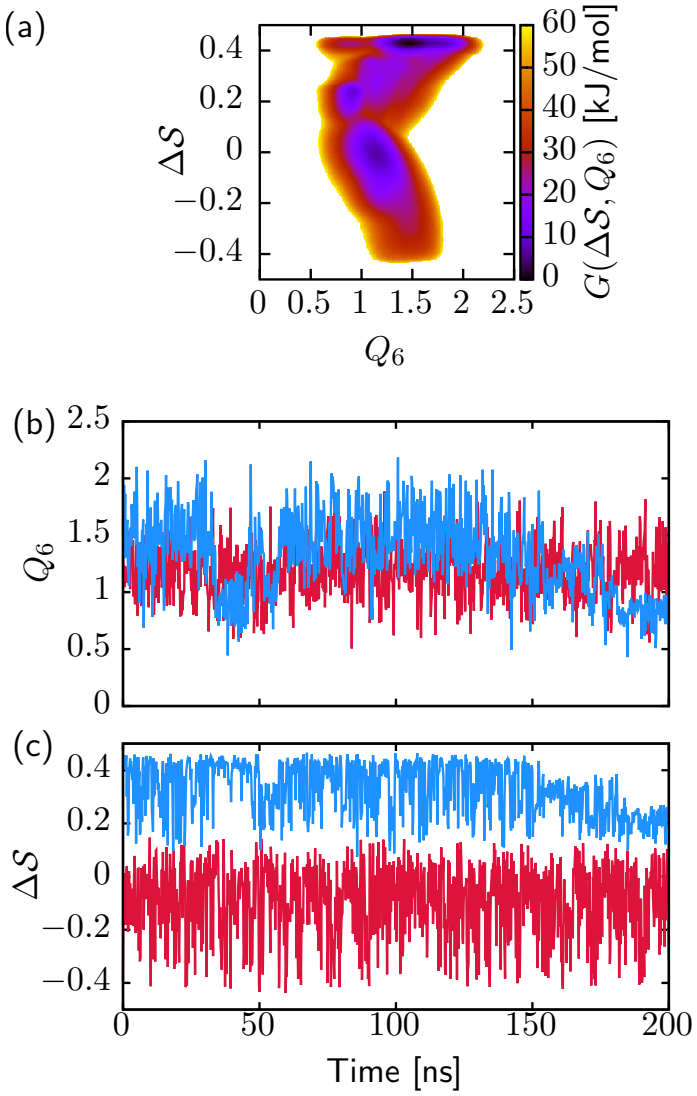

Figure S4: Two-dimensional CV-space: Q_6 & $\Delta\mathcal{S}$. (a) Two-dimensional free energy landscape calculated from the Metadynamics simulations. The time evolution of the CVs during the simulations: (b) Q_6; (c) $\Delta\mathcal{S}$. There is no transition between α and β forms.

- $N^{\mathrm{mon}} = 14$, $N^{\mathrm{chain}} = 12$: temperature $T = 400$ K, simulation time $t = 2$ μs.
- $N^{\mathrm{mon}} = 10$, $N^{\mathrm{chain}} = 12$: temperature $T = 600$ K, simulation time $t = 1$ μs.
- $N^{\mathrm{mon}} = 10$, $N^{\mathrm{chain}} = 36$: temperature $T = 600$ K, simulation time $t = 0.5$ μs.

4.1 Quantum-chemical methods

Phonon modes are computed to confirm the stationary points as local minima and to give access to temperature-dependent harmonic enthalpy (H^{HA}) and Gibbs free energy (G^{HA})

$$H^{\mathrm{HA}}(T,P) = E_{\mathrm{latt}} + H^{\mathrm{HA}}_{\mathrm{vib}}(T) + PV\,, \tag{S6}$$

$$G^{\mathrm{HA}}(T,P) = E_{\mathrm{latt}} + G^{\mathrm{HA}}_{\mathrm{vib}}(T) + PV\,. \tag{S7}$$

Here, E_{latt} is the zero-temperature internal energy of the crystal given per monomer unit. The vibrational internal energy contributions are

$$H^{\mathrm{HA}}_{\mathrm{vib}}(T) = \sum_{\mathbf{k},p}\left[\frac{\hbar\omega_{\mathbf{k},p}}{2} + \frac{\hbar\omega_{\mathbf{k},p}}{\mathrm{e}^{-\frac{\hbar\omega_{\mathbf{k},p}}{k_{\mathrm{B}}T}} - 1}\right] \tag{S8}$$

and the vibrational contributions to the Gibbs free energy are

$$G^{\mathrm{HA}}_{\mathrm{vib}}(T) = \sum_{\mathbf{k},p}\frac{\hbar\omega_{\mathbf{k},p}}{2} + k_{\mathrm{B}}T\sum_{\mathbf{k},p}\left[\ln\left(1 - \mathrm{e}^{-\frac{\hbar\omega_{\mathbf{k},p}}{k_{\mathrm{B}}T}}\right)\right]\,. \tag{S9}$$

The phonon frequencies $\omega_{\mathbf{k},p}$ correspond to a $\mathbf{k}$-point in first Brillouin zone and a phonon band index p.

References

[1] Alessandro Laio and Michele Parrinello. Escaping free-energy minima. *Proceedings of the National Academy of Sciences*, 99(20):12562–12566, 2002.

[2] Alessandro Barducci, Massimiliano Bonomi, and Michele Parrinello. Metadynamics. *Wiley Interdisciplinary Reviews: Computational Molecular Science*, 1(5):826–843, 2011.

[3] Cameron Abrams and Giovanni Bussi. Enhanced sampling in molecular dynamics using metadynamics, replica-exchange, and temperature-acceleration. *Entropy*, 16(1):163–199, 2014.

[4] Alessandro Barducci, Giovanni Bussi, and Michele Parrinello. Well-tempered metadynamics: a smoothly converging and tunable free-energy method. *Physical review letters*, 100(2):020603, 2008.

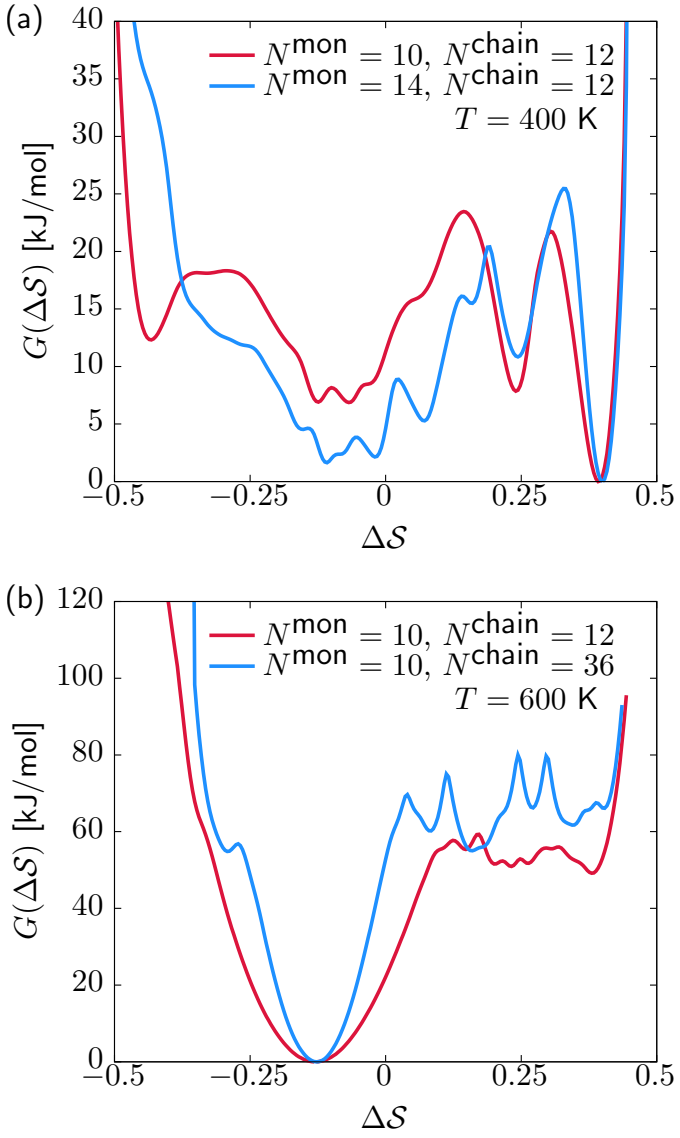

Figure S5: Free-energy profiles as a function of $\Delta\mathcal{S}$ for different system sizes. (a) Change in the number of monomers per chains, simulated at $T = 400$ K; (b) change in the number of chains, simulated at $T = 600$ K.

[5] James F Dama, Michele Parrinello, and Gregory A Voth. Well-tempered metadynamics converges asymptotically. *Physical review letters*, 112(24):240602, 2014.

[6] Pratyush Tiwary and Michele Parrinello. A time-independent free energy estimator for metadynamics. *The Journal of Physical Chemistry B*, 119(3):736–742, 2014.

[7] Alessandro Laio and Francesco L Gervasio. Metadynamics: a method to simulate rare events and reconstruct the free energy in biophysics, chemistry and material science. *Reports on Progress in Physics*, 71(12):126601, 2008.

[8] Paul J Steinhardt, David R Nelson, and Marco Ronchetti. Icosahedral bond orientational order in supercooled liquids. *Physical Review Letters*, 47(18):1297, 1981.

[9] Paul J Steinhardt, David R Nelson, and Marco Ronchetti. Bond-orientational order in liquids and glasses. *Physical Review B*, 28(2):784, 1983.